# ITER PREDICTIONS USING THE GYRO VERIFIED AND EXPERIMENTALLY VALIDATED TGLF TRANSPORT MODEL

by
J.E. KINSEY, G.M. STAEBLER, J. CANDY
and R.E. WALTZ

**GENERAL ATOMICS**

# DISCLAIMER

GA–A26874

# ITER PREDICTIONS USING THE GYRO VERIFIED AND EXPERIMENTALLY VALIDATED TGLF TRANSPORT MODEL

by
J.E. KINSEY, G.M. STAEBLER, J. CANDY
and R.E. WALTZ

GENERAL ATOMICS PROJECT 03726
NOVEMBER 2010

**GENERAL ATOMICS**

# ITER Predictions Using the GYRO Verified and Experimentally Validated TGLF Transport Model

J.E. Kinsey, G.M. Staebler, J. Candy, and R.E. Waltz

General Atomics, P.O. Box 85608, San Diego, California 92186

e-mail contact of main author: kinsey@fusion.gat.com

**Abstract.** The trapped gyro-Landau fluid (TGLF) transport model computes the quasi-linear particle and energy driftwave fluxes in tokamaks with shaped geometry, finite aspect ratio, and collisions. The TGLF particle and energy fluxes have been successfully *verified* against a large database of collisionless nonlinear gyrokinetic simulations using the GYRO code. Using a new collision model in TGLF, we find remarkable agreement between the TGLF quasi-linear fluxes and 64 new GYRO nonlinear simulations with electron-ion collisions. In validating TGLF against DIII-D and JET H-mode and hybrid discharges we find the predicted temperature profiles are in excellent agreement with the measured ion and electron temperature profiles. ITER projections using TGLF show that the fusion gains are somewhat more pessimistic than the previous GLF23 results primarily due to finite aspect ratio effects included only in TGLF. The ITER results are sensitive to the improvements in the TGLF collision model while the results for DIII-D and JET hybrids are not. A new steady-state transport code TGYRO can evolve temperature and density profiles to match power and particle sources using local flux tube nonlinear GYRO simulations or a model like TGLF. TGYRO thus provides a critical *verification* of the TGLF predictions for ITER using GYRO.

## 1. Introduction

A new physics based driftwave model has been developed called the Trapped Gyro-Landau Fluid (TGLF) model [1, 2]. TGLF is an eigenvalue code that solves a set of 15–moment GLF equations and includes the effects of shaped geometry via the Miller equilibrium model [3], trapped particle physics, collisions, $E \times B$ shear, and a wider spectrum than its predecessor (GLF23) [4] spanning from long wavelength ITG/TEM modes to short wavelength ETG modes. TGLF uses four Hermite basis functions, solving a $120 \times 120$ complex matrix to find the eigenvalues for each toroidal mode number. GLF23 uses a parametrized trial wave function and solves a much smaller $8 \times 8$ matrix for each low-k mode and a $4 \times 4$ matrix for each high-k mode. While GLF23 successfully reproduced the profiles from a wide variety of tokamak discharges [5], it assumed infinite aspect ratio shifted circle geometry. TGLF is the first comprehensive driftwave transport model valid for finite aspect ratio shaped geometry. The quasilinear transport fluxes are computed using a saturation rule that is local in wavenumber and uses the two most unstable linear eigenmodes for each wavenumber. The philosophy behind the development of TGLF has been to formulate a reduced gyro-Landau-fluid model that accurately describes the fundamental physics of turbulent driftwave transport and is well *verified* against linear and nonlinear gyrokinetic turbulence simulations. We find the TGLF quasi-linear transport fluxes are a much better fit to nonlinear GYRO simulations than GLF23. To confidently predict the core confinement in ITER [6], we a need comprehensive physics based model of turbulent transport that is also well *validated* against experimental data.

We first summarize the results of verifying TGLF against nonlinear GYRO [7, 8] simulations followed by the results of validating the model against experimental profile data including the DIII-D tokamak [9]. Finally, we present the results from predictive

modeling studies of ITER using TGLF and verification using GYRO. The effects of finite aspect ratio are found to have important consequences on the predicted fusion performance of ITER. An update of the TGLF collision model also has an impact on the predictions. Density peaking and finite $\beta$ effects are both found to be beneficial. Since the predicted fusion performance is known to be sensitive to the temperature and density at the top of the H-mode pedestal we show the fusion predictions for ITER over a range in pedestal parameters.

## 2. Verification of TGLF Using GYRO Nonlinear Simulations

Model verification has played an essential role in the development of TGLF in an effort to accurately describe the linear growth rates and transport fluxes found in gyrokinetic turbulence simulations. We first used the GKS gyrokinetic stability code [10] to verify the linear growth rates and obtained average RMS error of 11.4% for a database of 1799 linear growth rates [11]. The quasilinear saturation rule in TGLF was then determined using 82 nonlinear GYRO gyrokinetic simulations of ITG/TEM modes using Miller geometry [2]. While the 82 GYRO simulations included shaped Miller geometry they did not include the effect of collisions. Recently, a new collision model was implemented in TGLF that was fit to numerical solutions of the gyrokinetic equation with pitch angle scattering of electrons. TGLF with the new collision model (TGLF-09) was found to give much better agreement with GYRO collisional simulations. Comparing TGLF with a new GYRO database of 64 collisional simulations, the average RMS errors in $[\chi_i, \chi_e]$ dropped from $[0.24, 0.27]$ to $[0.10, 0.13]$ going from the TGLF-APS07 model to the TGLF-09 model [12].
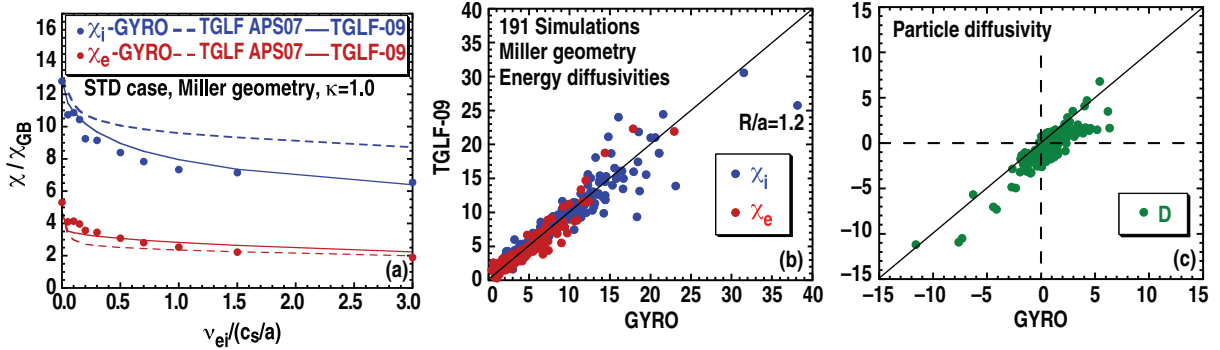


*FIG. 1.   (a) TGLF (solid, dashed lines) energy diffusivities and GYRO results (points) vs. $\nu_{ei}/(c_s/a)$ for the STD case with Miller geometry, $\kappa = 1.0$, and $s_\kappa = 0.0$. The vertical dashed lines denote the predicted values for ITER and DIII-D. TGLF-09 vs. GYRO (b) ion (blue) and electron (red) energy diffusivities and (c) particle diffusivity for 191 cases with Miller geometry.*

Figure 1(a) compares the TGLF and GYRO ion and electron energy diffusivities for a collisionality scan around the STD case with Miller geometry, $\kappa = 1.0$, $\delta = 0.0$, and $k_\theta \rho_s \leq 0.75$. With finite levels of electron-ion collisions, the energy fluxes from TGLF-09 are lower (especially for the ions) than those from TGLF-APS07 and show better agreement with GYRO. Figures 1(b,c) compare the diffusivities from TGLF-09 against those in our GYRO transport database of 191 nonlinear simulations including the 65 of the cases with electron-ion collisions. All the cases used Miller geometry and are electrostatic. The RMS errors averaged over the 11 scans with collisions in the database for $[\chi_i, \chi_e, D]$ are $[0.13, 0.16, 0.78]$ for TGLF-09 compared to $[0.24, 0.23, 0.98]$ for TGLF-APS07.

## 3. Validation of TGLF: Transport Modeling of Experimental Profiles

The TGLF-09 model has been validated against a large profile database of 133 L- and H-mode discharges from the DIII-D, JET, and TFTR tokamaks. The rms error in the incremental stored energy $W_{inc}$ (energy above the boundary location) is $\Delta R_W = 20\%$ for TGLF-09 which is lower than $\Delta R_W = 32\%$ obtained using GLF23. The effective offset for TGLF is $\langle R_W \rangle - 1 = 2\%$ while GLF23 has a value of $\langle R_W \rangle - 1 = -17\%$ (underpredicted). Figure 2(a) shows the predicted versus experimental $W_{inc}$ using the TGLF-09 model.
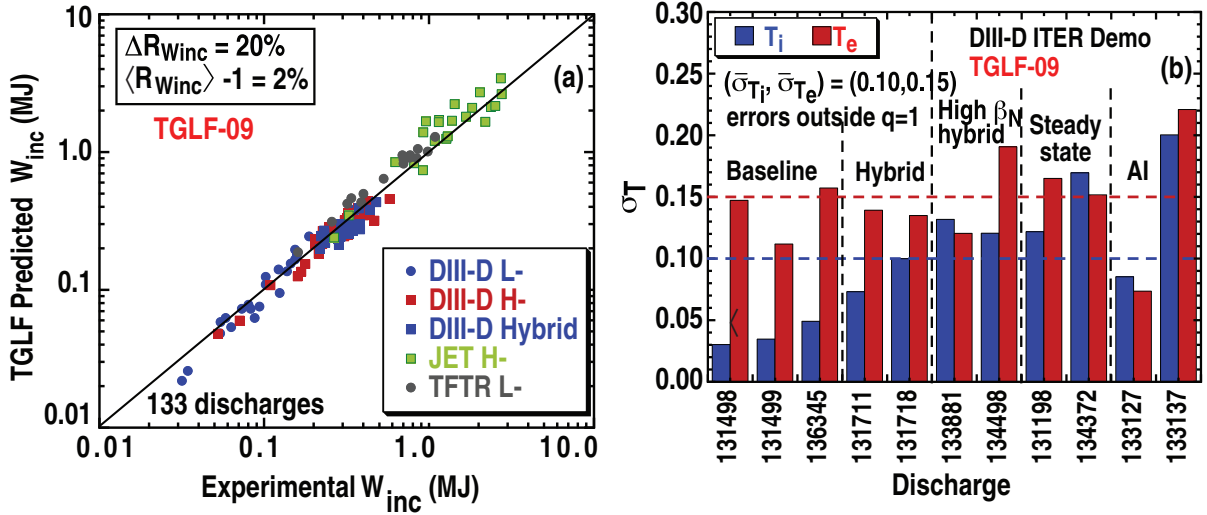


FIG. 2. (a) Predicted incremental stored energy $W_{inc}$ from the TGLF-09 model vs. experimental $W_{inc}$ for 133 DIII-D, JET, and TFTR L- and H-mode discharges. (b) RMS error in $T_i$ (blue) and $T_e$ for 11 DIII-D ITER demo discharges using TGLF-09.

Included are 25 DIII-D L-mode discharges (DB1), 33 DIII-D H-mode discharges (DB2), 22 JET H-mode discharges (DB4), and 16 TFTR L-mode discharges (DB9). Examination of the local figures of merit (the rms error $\sigma_T$ and offset $f_T$) shows that TGLF-09 exhibits better agreement with the temperature profiles for all 133 discharges than the GLF23. The average rms errors in $[T_i, T_e]$ are $[15\%, 16\%]$ for TGLF-09 and $[21\%, 23\%]$ for GLF23. The average offsets are $[0.003, 0.02]$ for TGLF-09 and $[-0.05, -0.10]$ for GLF23. Here, we predicted the temperature profiles using the XPTOR transport code with the same methodology described in Ref. [2]. The results for TGLF-APS07 are nearly identical to the TGLF-09 results because the change in the collision model mainly impacts the very low-k modes which tend to be quenched by $E \times B$ shear effects in most of discharges in the database. This is not found to be the case in our ITER predictions.

TGLF-09 has also been validated against recent DIII-D experiments designed to evaluate the four primary ITER operational scenarios incorporating the same shape and aspect ratio as ITER [13]. Overall, we find the level of agreement with the profiles from these ITER shaped discharges is as good as what was obtained in the 133 discharge database study. The one exception is discharge #133137 where TGLF-09 underpredicts both temperature profiles. Figure 2(b) shows the rms errors in the temperature profiles for 11 DIII-D ITER demo discharges. Here, the four ITER scenarios include the baseline conventional ELMy H-mode scenario, which targets $Q = 10$ at a plasma current of 15 MA  the hybrid scenario, which targets high neutron fluence at a reduced current of 12.5 MA  the steady-state scenario, which seeks fully noninductive operation at 9 MA with $Q \approx 5$; and the advanced inductive (AI) scenario which targets high fusion gain by optimizing high plasma current operation with increased MHD stability limits characteristic of hybrids.

The rms error $\sigma_T$ and offset $f_T$ between the predicted and experimental temperature profile for a given discharge are computed using the ITER Profile Database [14] definition,

$$\sigma_{\mathrm{T}} = \sqrt{\frac{1}{N} \sum_j \epsilon_j^2} \Bigg/ \sqrt{\frac{1}{N} \sum_j T_{\mathrm{x,j}}^2} \qquad\qquad f_{\mathrm{T}} = \frac{1}{N} \sum_{j=1}^{N} \epsilon_j \Bigg/ \sqrt{\frac{1}{N} \sum_j T_{\mathrm{x,j}}^2}$$

where $\epsilon_j = T_{\mathrm{s,j}} - T_{\mathrm{x,j}}$ is the deviation between the $j$th radial simulation point $T_{\mathrm{x,j}}$ and the corresponding experimental point $T_{\mathrm{s,j}}$ and $T$ is the local ion or electron temperature. The rms error quantifies the scatter of the simulated profile about the experimental data normalized to an average value. The offset provides a measure of the amount by which the overall simulated profile needs to be shifted downward (positive) or upward (negative) in order to minimize $\sigma_T$.

## 4. ITER Predictions

The fusion performance has been assessed for the ITER 15 MA conventional ELMing H-mode scenario [6] using the TGLF and GLF23 models. The TGLF predicted fusion power is more pessimistic than the GLF23 results primarily due to finite aspect ratio effects included only in TGLF. Figure 3(a) shows the predicted fusion power $P_{\mathrm{fus}}$ versus pedestal temperature ($T_{\rho=0.95}$) at fixed pedestal density using the TGLF and GLF23 models for an ITER conventional H-mode scenario with a somewhat flat prescribed density profile ($n_{\mathrm{e0}}/n_{\mathrm{ped}} = 1.1$) and an auxiliary heating power of $P_{\mathrm{aux}} = 30$ MW (20 MW of ICRH and 10 MW of NBI). The vertical dashed lines denote the pedestal temperatures yielding a target fusion gain of $Q = P_{\mathrm{fus}}/P_{\mathrm{aux}} = 10$. Using TGLF-09, the required value for $Q = 10$ is $T_{\mathrm{ped}} = 5.1$ keV corresponding to $\beta_{\mathrm{ped,N}} = 0.92$. The ITER parameters we used are $R = 6.2$ m, $a = 2.0$ m, $I_p = 15$ MA, $B_T = 5.3$ T, $\kappa = 1.75$, $Z_{\mathrm{eff}} = 1.7$, and $M_i = 2.5$.
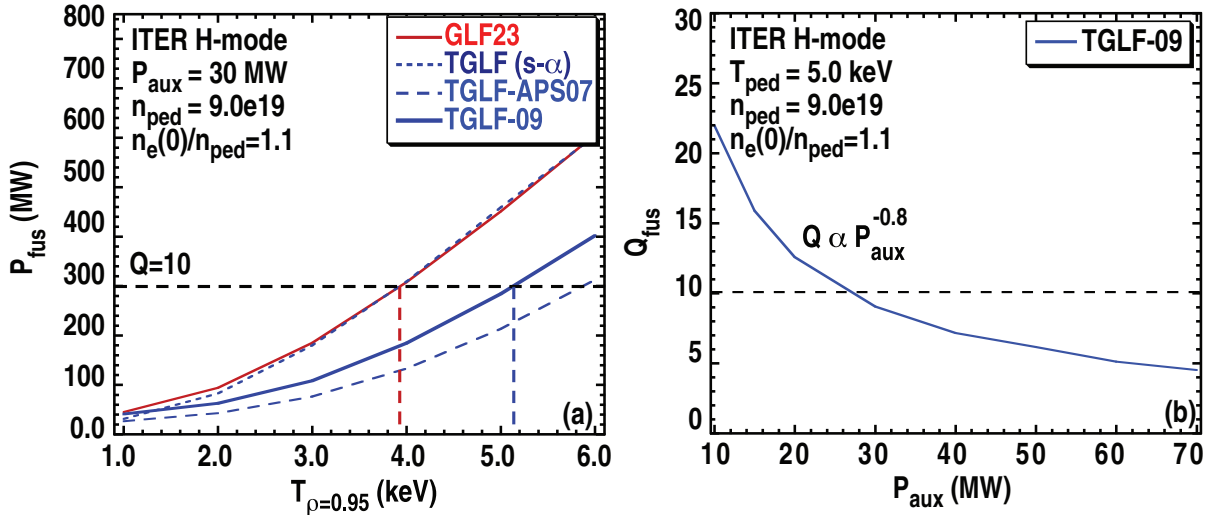


FIG. 3. (a) Predicted fusion power for a conventional H-mode ITER scenario with $P_{\mathrm{aux}} = 30$ MW and a prescribed density profile with $n_{\mathrm{e0}}/n_{\mathrm{ped}} = 1.1$ ($\bar{n}_e/n_{\mathrm{GW}} = 0.8$) using the TGLF and GLF23 models. (b) Fusion Q vs. auxiliary power for the case with $T_{\mathrm{ped}} = 5.0$ keV.

Using infinite aspect ratio shifted circle geometry ($s-\alpha$), TGLF gives the same results as GLF23. When finite aspect ratio Miller geometry is used in TGLF, the ITG/TEM transport increases (mainly $\chi_e$) causing the predicted $P_{\mathrm{fus}}$ to decrease (see the TGLF-APS07 results). Changes in the TGLF collision model also have an impact. Using the new collision model in TGLF (TGLF-09) results in an increase in $P_{\mathrm{fus}}$ relative to the

TGLF-APS07 results but still below the GLF23 results. Above $T_{\mathrm{ped}} = 2$ keV, the TGLF-09 results scale like $T_{\mathrm{ped}}^2$ (or $\beta_{\mathrm{ped}}^2$) which is characteristic of a stiff transport model.

Stiff turbulent transport has important consequences on the fusion performance in ITER. Due to the stiff nature of TGLF, the temperature profiles are insensitive to changes in the amount of $P_{\mathrm{aux}}$ so that fusion $Q$ scales like $1/P_{\mathrm{aux}}^{0.8}$ for a fixed $\beta_{\mathrm{ped}}$ as shown in Fig. 3(b). Increasing $P_{\mathrm{aux}}$ while holding the $\beta_{\mathrm{ped}}$ fixed only slightly raises $P_{\mathrm{fus}}$ while reducing the fusion $Q$. Increasing the fusion power beyond the baseline prediction with additional $P_{\mathrm{aux}}$ is difficult. A positive consequence of stiff transport is that $P_{\mathrm{aux}}$ can be reduced with little decrease in $P_{\mathrm{fus}}$. So, increasing the fusion $Q$ can be achieved by reducing $P_{\mathrm{aux}}$ while maintaining enough heating to remain above the H-mode power threshold.

In our ITER modeling the $T_i$ and $T_e$ profiles are predicted taking the equilibrium, energy and particle sources and sinks from the output of a TRANSP simulation [15]. The density, fast ion, and $Z_{\mathrm{eff}}$ profiles are held fixed and the toroidal rotation is assumed to be zero. The boundary conditions are enforced at a normalized toroidal flux of $\hat{\rho} = 0.95$ with $T_{\mathrm{e,BC}} = T_{\mathrm{i,BC}}$. When we reference $T_{\mathrm{ped}}$ we are referring to the $\hat{\rho} = 0.95$ location. The predicted temperatures are evolved to a steady-state solution of the transport equations using a fully implicit Newton solver in the XPTOR transport code. The fusion power, ohmic heating, bremstrahlung and synchrotron radiative losses are computed self-consistently assuming an effective main ion mass of $A = 2.5$ (50-50 DT ion mixture) and a single carbon impurity species.

## A    Sensitivity to ETG modes and density peaking

Recent TGLF modeling studies have shown that ETG transport can dominate the electron energy transport in DIII-D hybrid discharges where $E \times B$ shear effects have quenched the low-k modes [12]. But, there is some uncertainty in how large the high-$k$ saturation levels should be in TGLF when Miller geometry is used. The ETG contribution to $\chi_e$ in TGLF (above $k_\theta \rho_s = 1.0$) was calibrated to yield a ratio of $\chi_{\mathrm{high-k}}/\chi_{\mathrm{e,low-k}} \simeq 0.12$ to match a single coupled low/high-k GYRO simulation of the GA-STD case assuming shifted circle geometry and a reduced mass ratio of $\mu = \sqrt{m_i/m_e} = 30$ [2, 16]. Comparable coupled low/high-$k$ GYRO nonlinear simulations with Miller geometry have yet to be performed.

The predicted fusion power in ITER is found to be relatively insensitive to the ETG transport levels in TGLF. Several reference H-mode cases were considered where the ETG transport was eliminated from the TGLF spectrum. Figure 4(a) shows the predicted TGLF energy diffusivities for case with $P_{\mathrm{aux}} = 50$ MW, $n_{e0}/n_{\mathrm{ped}} = 1.3$, $T_{\mathrm{ped}} = 5.0$ keV, and $n_{\mathrm{ped}} = 8.0 \times 10^{19}\ m^{-3}$. Here, the ETG modes contribute approximately 30% to the total $\chi_e$. On average, $P_{\mathrm{fus}}$ increases by only $\approx 5\%$ when ETG modes are removed from the TGLF spectrum compared to the baseline result with ETG modes. As the ETG transport is reduced, the temperature gradients increase driving the ITG/TEM modes more unstable. As a result, there is very little decrease in the total energy transport when the mixture of low/high-k mode is varied. So, if $E \times B$ shear effects are weak in ITER, then it appears that the accuracy of ETG transport is not important.

At fixed $\beta_{\mathrm{ped}}$, we find moderate density peaking improves ITER performance by about 5% above the baseline case with a flat density profile. While we have not considered impurity and/or helium ash accumulation, a higher reactivity is evident and fairly robust. Figure 4(b) shows the fusion power versus $T_{\mathrm{ped}}$ for 3 different prescribed $n_e$ profiles with varying peaking factors. TGLF predictions of the density profile yields peaking factors of $n_{e0}/n_{\mathrm{ped}} = 1.3$ as shown by the red dots. Peaked density profiles with $n_{e0}/n_{\mathrm{ped}} \geq 1.3$ have been observed in low collisionality AUG, JET, and C-mod H-mode plasmas [17, 18, 19].
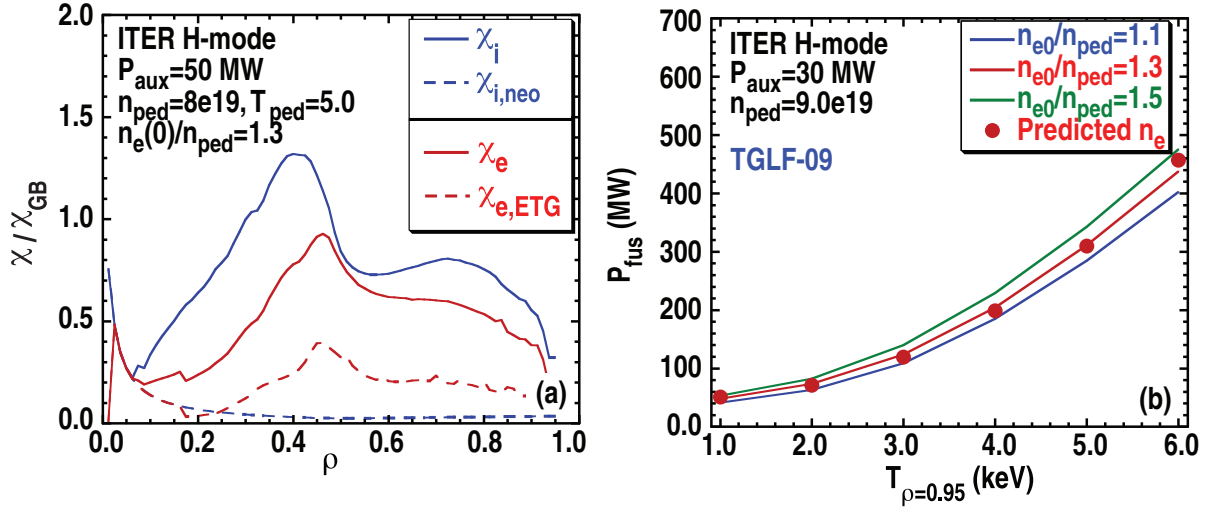
FIG. 4. (a) TGLF-09 ion (blue) and electron (red) energy diffusivities versus $\hat{\rho}$ for an ITER ELMy H-mode scenario. The dashed red and blue lines denotes the high-k part of $\chi_e/\chi_{GB}$ and the neoclassical energy diffusivity, respectively. (b) Predicted fusion power versus $T_{ped}$ for various density peaking factors for the same ITER scenario with 30 MW of auxiliary heating using the TGLF-09 model. The points indicate the results where the density profile was predicted.

Including finite $\beta$ effects in TGLF also leads to a 5% increase in $P_{fus}$. In low to moderate $\beta_N$ DIII-D and JET cases we have found finite $\beta$ effects to be mildly stabilizing. Using a small level of toroidal rotation, as predicted by GLF23 in predictive TRANSP runs [15], also produces a 5% increase in $P_{fus}$ due to $E \times B$ shear stabilization. While the individual benefits of density peaking, finite $\beta$, and $E \times B$ shear from small toroidal rotation $v_\phi$ are not large, the combined increase in $P_{fus}$ is $\approx 60\%$ above the conservative base case with 285 MW. Table I summarizes the results of including density peaking, finite $\beta$, and finite $v_\phi$ for the $T_{ped} = 5.0$ keV case shown in Fig. 3(a) using TGLF-09. The EPED model [20, 21] predicts a pedestal height at the boundary condition specified (two half widths in from the center of the edge barrier) in the range $\beta_{ped,N} = 0.74 - 0.92$, depending on the input value of pedestal density and global $\beta$. By optimizing over these quantities, the value of $\beta_{ped,N} = 0.9$ needed for the case in Table I can be achieved.

Table 1. ITER performance using TGLF-09 for a conventional H-mode scenario with $P_{aux} = 30$ MW, $v_\phi = 0$, $n_{e0}/n_{ped} = 1.1$, $T_{ped} = 5.0$ keV, $n_{ped} = 9.0 \times 10^{19}$ $m^{-3}$, $\beta_{ped,N} = 0.9$.

| Scenario variation | $P_{fus}$ (MW) |
|---|---|
| Base case with prescribed $n_e$ ($n_{e0}/n_{ped} = 1.1$) | 285 |
| Predicted density with $n_{e0}/n_{ped} = 1.3$ | 310 |
| Finite $\beta$ with prescribed $n_e$ ($n_{e0}/n_{ped} = 1.1$) | 311 |
| Predicted $n_{e0}/n_{ped} = 1.3$, Finite $\beta$ | 373 |
| Predicted $n_{e0}/n_{ped} = 1.3$, Finite $\beta$, $v_{\phi,0} = 0.5 \times 10^5$ (m/s) | 452 |

## 5. Verification of the TGLF ITER results against GYRO using TGYRO

The TGYRO code has been used as an additional tool for verifying the XPTOR/TGLF results. Our goal is verify the TGLF ITER predictions obtained using the XPTOR code against TGYRO predictions using local GYRO flux tube simulations to compute the turbulent energy transport. TGYRO is a steady state transport code which adjusts temperature, density and toroidal rotation profiles until the simulated flows match to

input source flows from the plasma center to the pedestal [22]. TGYRO can use either GYRO or TGLF to compute turbulent fluxes, thus providing a unified framework for TGLF-GYRO verification and validation of both with experimental data. TGYRO can also call the NEO code to compute self-consistent, first-principles neoclassical fluxes, poloidal flows and bootstrap current in general geometry [23].
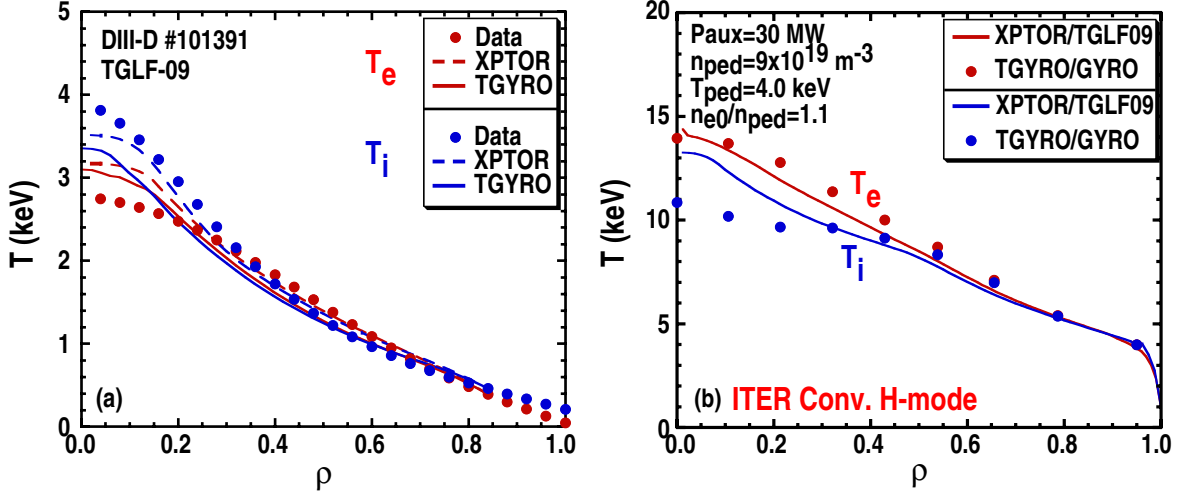


FIG. 5. (a) TGLF-09 predicted temperatures for DIII-D #101391 using the XPTOR (dashed lines) and TGYRO (solid lines) codes. (b) Predicted temperatures for an ITER H-mode scenario with no dilution using XPTOR/TGLF-09 and TGYRO/GYRO.

The results of code benchmarking TGYRO against XPTOR using TGLF-09 for a DIII-D L-mode are shown in Fig. 5. The agreement is excellent assuming no dilution. Figure 5(b) shows the TGYRO/GYRO results compared to the XPTOR/TGLF-09 results for the ITER case in Fig. 3(a) with $T_{\text{ped}} = 4.0$ keV and no dilution. In TGYRO, GYRO flux tube simulations were performed at 8 radial zones with 8 toroidal modes, $\hat{k}_y \leq 0.70$, and a box size of $[L_x/\rho_s, L_y/\rho_s] = [64, 64]$. The GYRO results are in good agreement with the TGLF-09 results, thus providing confidence in our ITER predictions.

## 6. Summary

The results can be summarized as follows:

1. TGLF has been verified against 191 nonlinear GYRO simulations. The database RMS errors for $[\chi_i, \chi_e, D]$ are $[0.13, 0.16, 0.78]$ for TGLF-09 (w/ new collision model) compared to $[0.24, 0.23, 0.98]$ for TGLF-APS07 (with old collision model).

2. TGLF accurately predicts both the electron and ion temperature profiles with average RMS values in $[T_i, T_e]$ of [15%,16%] for 133 L- and H-mode discharges from DIII-D, JET, and TFTR. GLF23 has rms errors of [21%,23%] .

3. Finite aspect ratio effects in TGLF (Miller geometry) cause the fusion projections in ITER to be lower than that for GLF23 (infinite aspect ratio, shifted circle geometry)

4. Because of the stiff transport properties of TGLF, the fusion $Q$ scales like $\beta_{\text{ped}}^2$ and also like $P_{\text{aux}}^{-0.8}$ at fixed pedestal $\beta$ (a perfectly stiff core scales like $Q \propto P_{\text{aux}}^{-1}$).

5. For small levels of $E \times B$ shear, the fusion power in ITER is sensitive to the choice of collision model in TGLF. Improving the collision model in TGLF raises the predicted fusion power closer to the GLF23 results compared to the TGLF-APS07 results.

6. Three ingredients for improving ITER performance have been identified including density peaking, finite $\beta$, and $E \times B$ shear due to finite toroidal rotation. Each improves $P_{fus}$ by 5%. Combined, they produce close to a 60% increase in $P_{fus}$ above the conservative baseline case to yield $Q = 15$ and $P_{fusion} = 452\,\mathrm{MW}$ at $\beta_{ped,N} = 0.9$.

7. The XPTOR/TGLF-09 results for ITER have been verified against the TGYRO code using GYRO nonlinear simulations for the energy transport.

8. The predictions in this paper are not the result of an optimization study of ITER.

In future work, there is a need to compare TGLF against nonlinear GYRO simulations with moderate to large values of $\beta$ and shaped geometry. The impact of electromagnetic effects on both the low-k and high-k modes needs to be examined especially for core plasma conditions with moderate to high $\beta$ values. We also plan on implementing momentum transport in TGLF and validating the predicted toroidal rotation profiles against experimental data. Historically, the focus has been on developing and testing core turbulence models. The results found here for DIII-D hybrids demonstrate the need to also develop improved models for neoclassical transport. We plan to implement the NEO code into the XPTOR transport code to be used in conjunction with the TGLF model.

## References

[1] STAEBLER, G.M., et al., Phys. Plasmas **14** (2007) 055909
[2] KINSEY, J.E., et al., Phys. Plasmas **15** (2008) 055908
[3] WALTZ, R.E. and MILLER, R.L., Phys. Plasmas **6** (1999) 4265
[4] WALTZ, R.E., et al., Phys. Plasmas **4** (1997) 2482
[5] KINSEY, J.E., Fusion Sci. Tech. **48** (2005) 1060
[6] SHIMADA, M., et al., Nucl. Fusion **47** (2007) S1
[7] CANDY, J. and WALTZ, R.E., J. Comput. Phys. **186** (2003) 545
[8] CANDY, J. and WALTZ, R.E., Phys. Rev. Lett. **91** (2003) 45001
[9] MAHDAVI, A. and LUXON, J.L., Fusion Sci. Tech. **48** (2005) 2
[10] KOTSCHENREUTHER, M., Bull. Am. Phys. Soc. **37** (1992) 1432
[11] STAEBLER, G.M., et al., , Phys. Plasmas **12** (2005) 102508
[12] KINSEY, J.E., et al., submitted to Phys. Plasmas (2010)
[13] DOYLE, E.J., et al., Nucl. Fusion **50** (2010) 075005
[14] ITER Physics Expert Groups on Confinement and Transport and Confinement Modeling and Database, Nucl. Fusion **40** (2000) 1955
[15] BUDNY, R.V., Nucl. Fusion **49** (2009) 085008
[16] WALTZ, R.E., et al., Phys. Plasmas **14** (2007) 056116
[17] ANGIONI, C., et al., Nucl. Fusion **47** (2007) 1326
[18] WEISEN, H., et al., Nucl. Fusion **45** (2005) L1
[19] GREENWALD, M., et al., Nucl. Fusion **47** (2007) L26
[20] SNYDER, P.B., et al., Phys. Plasmas **16** (2009) 056118
[21] SNYDER, P.B., et al., this conference, THS/1-1.
[22] CANDY, J., et al., Phys. Plasmas **16** (2009) 060704
[23] BELLI, E. and CANDY, J., Plasma Phys. Control. Fusion **50** (2008) 095010